minerals

MDPI

Article

Redox Conditions of the Late Ediacaran Ocean on the Southern Margin of the North China Craton

Jie Yang [1,2,*], Wei Jin [3,*], Guodong Wang [1], Le Wan [4] and Zuoxun Zeng [4]

[1] Shandong Provincial Key Laboratory of Water and Soil Conservation and Environmental Protection, School of Resources and Environment, Linyi University, Linyi 276000, China; wangguodong10@mails.ucas.ac.cn
[2] College of Earth Science and Engineering, Shandong University of Science and Technology, Qingdao 266590, China
[3] Wuhan Center of Geological Survey, China Geological Survey, Wuhan 430205, China
[4] School of Earth Sciences, China University of Geosciences, Wuhan 430074, China; wl@cug.edu.cn (L.W.); zuoxun.zeng@126.com (Z.Z.)
* Correspondence: jieyangucr@163.com (J.Y.); jinwei1961@163.com (W.J.)

Abstract: Previous studies have revealed dynamic and complex redox conditions of the late Ediacaran ocean. Integrated analyses of Ediacaran successions on different continents can help to better understand global ocean redox conditions. In this study, we used iron and redox-sensitive trace elements (RSTEs) geochemical analyses to present the detailed redox conditions of the late Ediacaran Dongpo Formation on the southern margin of the North China Craton (NCC). Paleoredox reconstruction reveals a dominantly anoxic late Ediacaran ocean punctuated by multiple transient oxygenation events across the southern margin of the NCC. These transient oxidation events in the NCC may have contributed to the appearance of the Ediacaran tubular fossil *Shaanxilithes*. Based on the assumption that local iron speciation data in a global framework can track the mean and variance of paleoredox conditions through time, we additionally analyzed about 3300 new and published iron speciation data from fine-grained clastic rocks to infer the global redox change in Ediacaran–Cambrian oceans. Our statistical analyses indicated dynamic Ediacaran marine redox conditions and stepwise early–middle Cambrian ocean oxygenation. The appearance and rise of the Ediacaran biota and the diversification of metazoans corresponded temporally with the middle Ediacaran global ocean oxygenation and the early–middle Cambrian stepwise oceanic oxygenation, respectively. Our results highlight the coevolutionary relationship between ocean redox conditions and early animals.

Keywords: iron speciation; ocean oxygenation; redox conditions; Ediacaran; North China Craton

check for updates

Citation: Yang, J.; Jin, W.; Wang, G.; Wan, L.; Zeng, Z. Redox Conditions of the Late Ediacaran Ocean on the Southern Margin of the North China Craton. *Minerals* **2023**, *13*, 1124. https://doi.org/10.3390/min13091124

Academic Editor: Hermann Kudrass

Received: 31 July 2023
Revised: 22 August 2023
Accepted: 22 August 2023
Published: 25 August 2023

Copyright: © 2023 by the authors. Licensee MDPI, Basel, Switzerland. This article is an open access article distributed under the terms and conditions of the Creative Commons Attribution (CC BY) license (https://creativecommons.org/licenses/by/4.0/).

1. Introduction

Because animals require free oxygen (O_2), understanding the cause-and-effect relationship between O_2 and life is important for deducing the early evolution of Earth's environments and animals [1]. The oxygenation of the Earth's atmosphere proceeded in two major episodes near the beginning of the Proterozoic Eon, known as the 'Great Oxidation Event' or GOE [2], and its end, known as the 'Neoproterozoic Oxidation Event' or NOE [3,4]. During the NOE, the Ediacaran period was a critical interval in the late Neoproterozoic, which witnessed the breakup of the Rodinia supercontinent, the climatic recovery after the 'Snowball Earth', and the assembly of Gondwanaland [5]. To better understand the ocean redox conditions under the impact of the NOE, previous studies have revealed the highly fluctuating and heterogeneous redox conditions of the global marine environment throughout the Ediacaran–Cambrian interval [6–8]. Presumably, the protracted rise of oxygen in the ocean and atmosphere during the late Ediacaran could oxygenate basins regionally, one after another [9]. Biological changes might have happened within these oxygenated basins under suitable environmental conditions. The relationship between environmental conditions and the evolution of early animals can be suggested by

comprehensive studies of paleontological, petrologic, geochemical, geochronological, and sequence stratigraphic analyses of global Ediacaran successions [10–13].

As mentioned above, integrated analyses of Ediacaran successions on different continents can help to better understand the global ocean redox conditions. The North China Craton (NCC) was suggested as being isolated at low latitudes of the Northern Hemisphere during the Ediacaran Period [14–17] (Figure 1A). The paleoredox conditions of the late Ediacaran ocean in the NCC are not well understood. Thus, detailed paleoredox reconstruction from successions on the NCC can fill in the blanks in global Ediacaran studies. To explore the marine redox structure of the NCC during the late Ediacaran, we analyzed iron-speciation and redox-sensitive trace metals for the fine-grained clastics of the Dongpo Formation from one fossiliferous Ediacaran section on the southern margin of the NCC. Combining this analysis with fossil record of the same section, we try to provide new insights into changes in marine redox conditions across the late Ediacaran and the potential links to early animal evolutions.

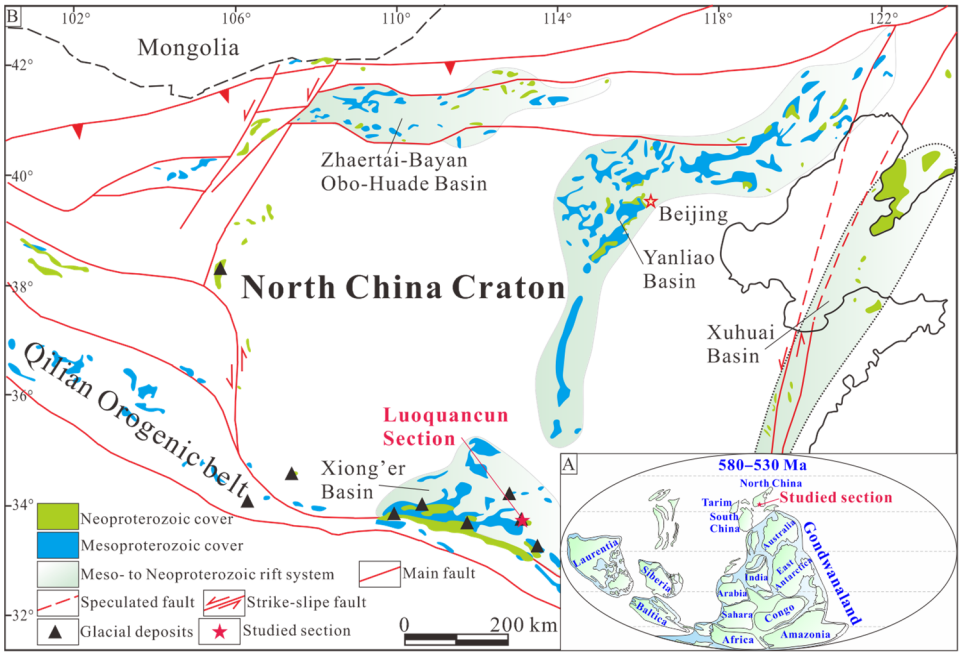


Figure 1. (**A**) Global paleographic reconstruction of late Ediacaran (580–530 Ma), modified from [15]; (**B**) simplified geological map showing the Meso-Neoproterozoic strata in the NCC, modified from [18,19].

2. Geological Background and Sampling

The NCC is one of the major Precambrian cratons in China, with a maximum age of ~3.8 Ga and an area of ~3 × 10^6 km^2 [20–23]. The Meso–Neoproterozoic strata are mainly deposited within the Xiong'er, Xuhuai, Yanliao, and Zhaertai-Bayan Obo-Huade basins [18,19,24,25] (Figure 1B). Widespread Cambrian transgressive successions disconformably overlie on these Meso–Neoproterozoic strata in the NCC, known as the 'Great Unconformity' [26]. Owing to the mid–late Neoproterozoic uplift of the NCC, the late Neoproterozoic strata in most of this continent were denuded. Following the subsequent northward transgression, the Ediacaran successions were mainly deposited on the southern margins of the NCC (Figure 1B), such as the Zhengmuguan and Dongpo formations on the southwestern margin [27–29], the Luoquan and Dongpo formations on the southern margin [30,31], and the Fengtai Formation on the southeastern margin.

The studied Luoquancun section is located at Luoquan Village, Mangchun Town, Linru County, in west Henan Province, on the southern margin of the NCC. It is the stratotype section of the Ediacaran Luoquan and Dongpo formations. In this section, the Ediacaran Luoquan Formation is conformably overlain by the Ediacaran Dongpo Formation and disconformably overlies the sandstone of the Mesoproterozoic Beidajian Formation. The

Luoquan Formation ranges from 20 to 200 m in thickness on the southern margin of the NCC and has a thickness of ~190 m in the study section. Here, the Luoquan Formation comprises upper stratified diamictites and lower massive diamictites (Figure 2C,E). Still higher, the *Shaanxilithes*-bearing Dongpo Formation is disconformably overlain by the trilobite-bearing sandstone of the Cambrian Xinji Formation (Figure 2A). The Dongpo Formation is made up of shale/siltstone (Figure 2B,D). The finding of the late Ediacaran fossil *Shaanxilithes* in the Dongpo Formation gives convincing evidence of the Ediacaran age of the Dongpo Formation [32] and correlates it with these fossiliferous formations, such as the Tuerkeng Formation of the southwestern NCC [33], Dengying Formation of South China [34], and Zhoujieshan Formation of Qaidam Block [35]. Previous researchers have well studied the biostratigraphy, lithostratigraphy, and detrital zircon geochronology of the Dongpo Formation [26,31] and the sedimentary environments and glacial characteristics of the Luoquan Formation [22,30,36–38]. Such studies have suggested that the Luoquan Formation was deposited in a lacustrine glacial or continental glacial to proglacial marine environment and that the overlying Dongpo Formation formed in a shallow marine environment [24,30,38]. In this study, we used iron and redox-sensitive trace elements (RSTEs) geochemical analyses of the Ediacaran Dongpo Formation to further decipher the redox conditions of the late Ediacaran ocean on the southern margin of the NCC.

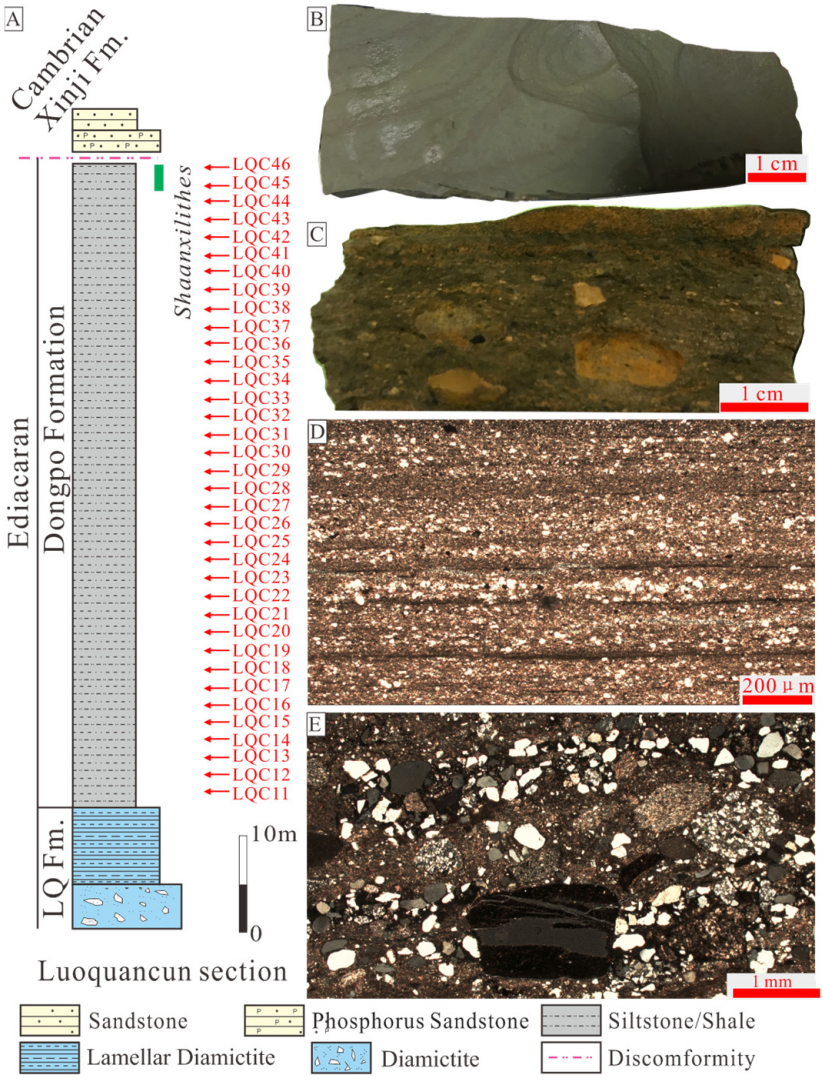


Figure 2. (**A**) Lithostratigraphic column of the study section; LQ Fm., Luoquan Formation; (**B**) hand specimen and (**D**) thin section of silty shale from the Dongpo Formation; (**C**) hand specimen and (**E**) thin section of diamictite from the Luoquan Formation.

Here, we focus on the Dongpo Formation, which is made up of shale/siltstone. The shale is made up of clay minerals and organic matter, and the siltstone consists of clay minerals, fragment quartz, and organic matter. In the study section, the total thickness of the Dongpo Formation is ~70 m, and most of the lamina are less than 1 mm. We collected thirty-six fresh samples from the Dongpo Formation for thin section and geochemical analyses.

3. Geochemical Methods

Thirty-six silty shales (LQC 11–46) of the Dongpo Formation were carefully collected at the Luoquancun section on the southern margin of the NCC. Redox-sensitive trace elements (RSTEs) were analyzed using a PerkinElmer Elan 9000 type inductively coupled plasma mass spectrometer (ICP-MS) at the Laboratory of ALS Chemex (Guangzhou). The enrichment factors (EFs) of the RSTEs were calculated as [El/$Al_{(sample)}$/El/$Al_{(reference)}$], where the reference is the values of average shale [39].

Iron (Fe) geochemical analyses were carried out at the State Key Laboratory of Biogeology and Environmental Geology, China University of Geosciences at Wuhan (SKLBEG, CUG). Iron contents in carbonates (Fe_{carb}), oxides (Fe_{ox}), and magnetite (Fe_{mag}) were measured following the standard iron sequential extraction procedure illustrated in [40], and iron in pyrite (Fe_{py}) was determined using the chromium reduction method [41]. Fe_{carb}, Fe_{ox}, and Fe_{mag} were sequentially extracted using sodium acetate, sodium dithionite, and oxalic acid–sodium oxalate. The extracted iron speciations were diluted and measured via atomic absorption spectrometry (AAS) with a relative standard deviation (RSD) lower than 5%. Fe_{py} was calculated based on pyrite-derived sulfur content, which was extracted and precipitated as Ag_2S. Sample powders were reacted with HCl and $CrCl_2$ to convert pyrite sulfur to H_2S and recovered as Ag_2S in silver nitrate traps.

4. Results and Discussion

4.1. Redox Conditions of the Late Ediacaran Ocean on the Southern Margin of the NCC

The iron and RSTEs geochemical data for the studied samples are listed in Table S1 (Supplementary Materials) and summarized in Figure 3. Based on observations of different iron phases in fine-grained siliciclastic rocks, iron geochemistry is commonly used as a paleoredox proxy to distinguish the local bottom water-column redox state of oxic, ferruginous (anoxic with dissolved ferrous Fe), and euxinic (anoxic with dissolved sulfide) [42,43]. Highly reactive iron (Fe_{HR}) includes iron that has been transformed to pyrite (Fe_{py}) and iron that can react with H_2S to form pyrite in the water column or during early sediment diagenesis, such as carbonate-associated iron (Fe_{carb}), ferric oxides (Fe_{ox}), and magnetite iron (Fe_{mag}) [44]. The other poorly or non-reactive iron (Fe_U) consists of iron in clay minerals and residual silicate-bound irons which are basically unreactive towards H_2S during deposition and early diagenesis [44]. In this scheme, $Fe_{HR} = Fe_{carb} + Fe_{ox} + Fe_{mag} + Fe_{py}$ and $Fe_T = Fe_{HR} + Fe_U$. The ratios of Fe_{HR}/Fe_T in modern and ancient sediments provide a threshold of 0.38 for the upper limit of oxic marine sediments, with Fe_{HR}/Fe_T values exceeding this threshold indicative of anoxia [42,43]. Under anoxic conditions ($Fe_{HR}/Fe_T > 0.38$), the ratios of Fe_{py}/Fe_{HR} can further distinguish the water column redox state as ferruginous ($Fe_{py}/Fe_{HR} < 0.7$–0.8) or euxinic ($Fe_{py}/Fe_{HR} > 0.7$–0.8). Because some non-redox processescan mute iron augmentation [45] and record lower Fe_{HR}/Fe_T ratios [43], a lower Fe_{HR}/Fe_T threshold value of <0.22 was suggested to interpret the oxic conditions, and Fe_{HR}/Fe_T values between 0.22 and 0.38 should be applied with caution [42,46]. Moreover, iron geochemistry is not appropriate for samples with $Fe_T < 0.5$ wt.%, which usually yield elevated Fe_{HR}/Fe_T values [47]. In this study, the total iron of all samples had an average weight of 3.41% with a minimum Fe_T value of 2.92% (LQC43), which exceeds the minimum request for iron geochemistry analysis, indicating that the Fe-speciation for these samples is suitable for redox reconstruction.

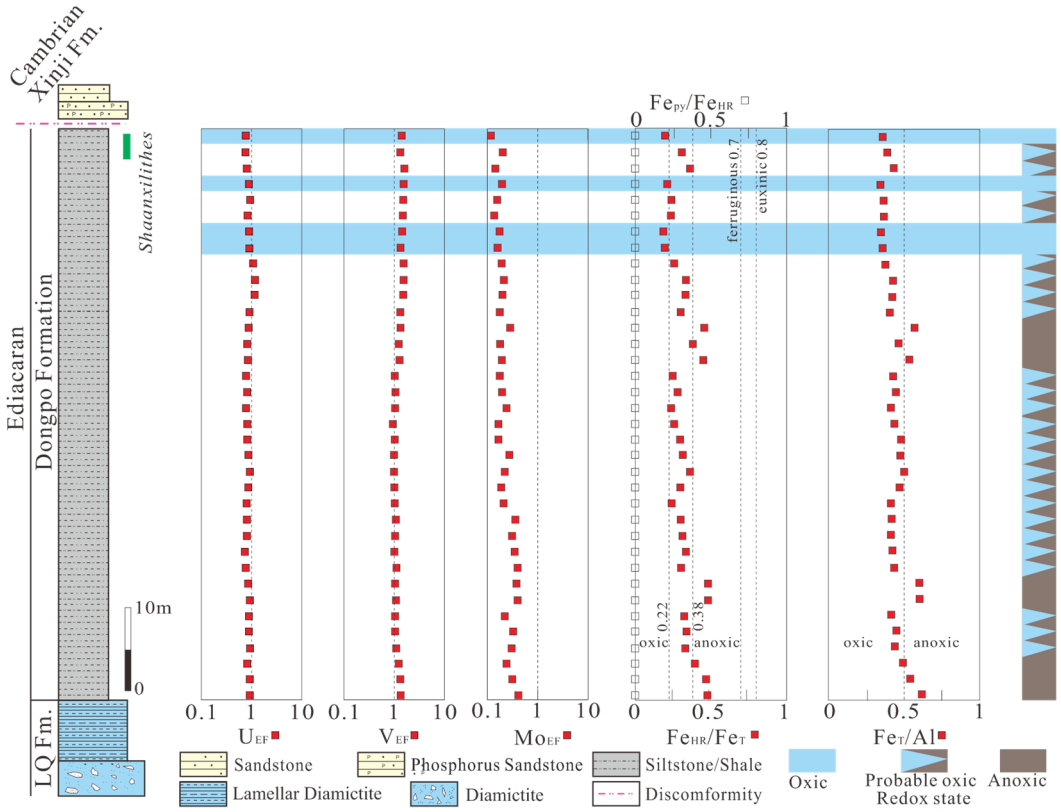


Figure 3. Chemostratigraphy of the Dongpo Formation at the Luoquancun section.

Because the Fe_{py} fraction is typically transformed into immobile iron oxides preserved near the original pyrite during chemical weathering and the Fe_{py}/Fe_{HR} and Fe_{HR}/Fe_T show no statistical correlation despite pyrite weathering [48,49], the Fe_{HR}/Fe_T is thought to be basically unaffected by modern oxidative weathering and can be used as a redox proxy despite evidence of secondary oxidative weathering [49]. The Fe_{HR}/Fe_T for the Dongpo Formation of the Luoquancun section ranges from 0.19 to 0.49 (mean = 0.33), fluctuating around the upper threshold of 0.38, and in combination with low Fe_{py}/Fe_{HR} ratios (~0), it revealed rapid oscillations between anoxic–ferruginous and oxic local bottom water column redox conditions (Figure 3). Considering that a part of the samples with Fe_{HR}/Fe_T ratios below 0.38 was plotted between 0.22 and 0.38, which also could be indicative of anoxic conditions, the measured iron speciation data, therefore, probably suggested a dominantly anoxic late Ediacaran ocean punctuated by multiple transient oxygenation events across the southern margin of the NCC.

The alternative redox proxy of total iron to aluminum (Fe_T/Al) can provide additional information on redox patterns. In the case of Fe_T/Al, crustal values of 0.5 ± 0.1 typically indicate oxic conditions and sediments deposited beneath anoxic water columns are specifically enriched in total iron, giving rise to Fe/Al enrichments above this threshold [10,45]. Therefore, the ratio of Fe_T/Al is widely used as an alternative redox proxy [10,44,50–52]. Samples from the Dongpo Formation give Fe_T/Al ratios from 0.35 to 0.61 (mean = 0.44), oscillating around a mean of 0.5. Samples with elevated Fe_T/Al ratios (>0.5), coupled with high Fe_{HR}/Fe_T ratios (>0.38), point to anoxic–ferruginous bottom water-column conditions. On the other hand, those samples with lower Fe_T/Al ratios (<0.5) are positively associated with lower Fe_{HR}/Fe_T ratios (<0.22–0.38), suggesting more oxygenated corresponding water column redox conditions (Figure 3).

Although the above analysis of iron geochemical data indicated anoxic–ferruginous depositional conditions for a portion of our samples, no significant RSTE enrichments (e.g., Mo, V, U) were observed in such samples (Figure 3). Samples with high Fe_{HR}/Fe_T ratios (>0.38) and low RSTE enrichments (EF < 1) are also found in the Doushantuo

Formation from the inner-shelf Jiuqunao and Jiulongwan sections in South China, which were interpreted as a consequence of the different sensitivities of iron speciation and RSTE to high-frequency redox variation in the Ediacaran ocean [53]. In theory, Mo enrichments require sulfide to convert soluble molybdate to thiomolybdates [54], but sulfide in the investigated sections is fairly low. Other redox-sensitive trace metals (e.g., V, U), which do not need sulfidic environments, usually exhibit low enrichments in the Proterozoic anoxic units [50,55]. It has been regarded as a consequence of widespread reducing sinks [50,56] or the small size of the corresponding oceanic trace metal reservoirs [57,58]. Compared with those classic Phanerozoic anoxic units, it is hard to separate the low Proterozoic enrichments from background levels [59]. Therefore, the absence of trace metal enrichments in our samples does not necessarily point to oxic conditions.

4.2. The Link between Ocean Redox Conditions and the Evolution of Early Animals

The present paleoredox reconstruction from the Luoquancun sections provides evidence of several marine shelf oxidation events in an anoxic late Ediacaran ocean along the southern margin of the NCC. However, the timing and magnitude of these oxidation events in the NCC and their temporal relationship with successions in other continents are uncertain. Previous studies have revealed a dominantly anoxic Ediacaran–early Cambrian ocean punctuated by multiple oceanic oxygenation events (OOEs) in the early (OOE1, ~632 Ma), middle (OOE2, ~580 Ma), and late (OOE3, ~560–541 Ma) Ediacaran and early Cambrian (OOE4) [55,60] (Figure 4C). Along with these OOEs, large-magnitude $\delta^{13}C$ excursions (Figure 4B) and key macrofossil assemblages (Figure 4A), including Avalon (~575–560 Ma), White Sea (~560–550 Ma), and Nama (~550–540 Ma) assemblages, occurred during the Ediacaran Period [61]. Because the studied sections are dominated by siliciclastic rocks that render a spotty $\delta^{13}C$ chemostratigraphic record, the correlation of the studied sections with $\delta^{13}C$ excursions in other Ediacaran successions is not straightforward [62].

The occurrence of the potential late Ediacaran index fossil *Shaanxilithes* from the Dongpo Formation probably constrains its depositional age to be late Ediacaran (~550–541 Ma) [31,35]. These fossils were found to be within the top of the Dongpo Formation, where oxygenations were persistent. Morphological and taphonomic reconstructions show that the body plan of the tubular fossil *Shaanxilithes* is close to the contemporaneous well-known skeletal fossil-*Cloudina*, which is a globally distributed eumetazoan and is well-preserved in the middle-upper part of the Dengying Formation in South China, the lower part of the Birba Formation in Southern Oman, and the lower Nama Group in southern Namibia [32,51]. Integrated data for I/[Ca + Mg], Ce/Ce*, and Fe-speciation analysis from the Nama Group indicated that the Nama Basin experienced intermittent anoxia and that the Nama skeletal communities were abundant in well-oxygenated environments but absent from oxygen-impoverished regions [51,63,64]. Such a phenomenon supports the prominent role of oxygen availability in controlling the distribution of Ediacaran skeletal metazoan communities [63,64]. Expanded anoxic conditions, recorded by $\delta^{238}U$ and $\delta^{34}S$, occurred after the first appearance of the skeletal fauna of the Nama Assemblage, demonstrating that the decline of the Ediacaran biota was unlikely to be driven by the expansion of anoxia in the Nama Basin [7,65]. Widespread oceanic anoxia and dynamic redox conditions at both temporal and spatial scales were also recorded in the fossiliferous Ediacaran successions in South China [8,66]. The Ediacaran biotas, as recorded in the Nama Assemblage, are spatiotemporally consistent with the episode of oceanic oxygenation, suggesting that the global oxygenations may have promoted the diversification of the Ediacaran biota [60,67,68].

Therefore, the iron geochemical data in this study revealed a dominantly anoxic late Ediacaran ocean punctuated by multiple transient oxygenation events across the southern margin of the NCC. This result reinforces previous studies' findings, based on analyses of C-S-N isotopes and trace elemental enrichments, that the Ediacaran Period was characterized by the pulsed oxygenation of a predominantly anoxic global ocean [5,69,70]. The new Fe_{HR}/Fe_T and Fe_T/Al data presented here suggest transient oxidation of shallow oceans during the deposition of the fossiliferous part of the Dongpo Formation. These transient

oxidation events in the NCC may have contributed to the appearance of the Ediacaran tubular fossil *Shaanxilithes*. Taken together, this study from the NCC combined with previous data from other Ediacaran successions (e.g., the Nama Group in Namibia, the Dengying Formation in South China, etc.) confirms a dominantly anoxic ocean punctuated by pulsed oxygenation events during the late Ediacaran and confirms that global oceanic oxygenation events may have contributed to the rise of the Ediacaran biota.

4.3. Statistical Analysis of Global Iron Speciation Data from the Ediacaran to Middle Cambrian

Although iron-based proxies only represent local redox conditions, these proxies still have important global implications when analyzed collectively and statistically [71]. Based on the assumption that local iron speciation data in a global framework can track the mean and variance of paleoredox conditions through time, we additionally integrated our iron speciation data from the NCC with published data from correlative sections in other continents for a global perspective on redox tracers. Following this template, we developed a data set of about 3300 new and published iron speciation data with $Fe_T > 0.5$ wt.% from fine-grained clastic rocks to infer the global redox change in Ediacaran–Cambrian oceans. Each sample was assigned a depositional environment and established age from its original literature or based on age constraints and sedimentation rates (Table S2, Supplementary Materials). The samples were binned into six relative age bins based on the major geological timescales. The Ediacaran was subdivided into the lower Ediacaran (635–580 Ma), middle Ediacaran (580–560 Ma), and upper Ediacaran (560–541 Ma), based on subdivision models in [62]. The Cambrian age bins were followed by the lower-middle Cambrian series as the Terreneuvian (541–521 Ma), Series 2 (521–509 Ma), and the Miaolingian (509–497 Ma).

The mean Fe_{HR}/Fe_T ratio in each time bin shows a dynamic variation in the Ediacaran time bins with mean Fe_{HR}/Fe_T ratios of 0.48, 0.39, and 0.51, respectively, and a progressive decline in the early–middle Cambrian with mean Fe_{HR}/Fe_T ratios declining from 0.60 in the Terreneuvian to 0.35 in the Miaolingian (Figure 4D), indicating dynamic Ediacaran marine redox conditions and stepwise oceanic oxygenation during the early–middle Cambrian. For the Ediacaran, the lowest mean Fe_{HR}/Fe_T ratios (0.39), the lowest proportion of anoxic samples (0.40), and the lowest proportion of euxinic samples (0.07) appeared in the middle Ediacaran (580–560 Ma), which may reflect the highest global ocean oxygenation level in the Ediacaran. These results have important implications for the evolution of early animals. It has been suggested that the Ediacaran biota appeared in the middle Ediacaran [72], reached their maximum taxonomic diversity at ~560 Ma, and then declined in the terminal Ediacaran stage (~550–541 Ma; Figure 4A) [67,73–75]. Our statistical analyses demonstrate that the appearance and rise of the Ediacaran biota correspond temporally with the global ocean oxygenation in the middle Ediacaran (580–560 Ma). Coincidentally, the largest $\delta^{13}C$ excursion (Shuram excursion, SE) in Earth history may also have occurred during this time period (Figure 4B). The coupled oceanic oxygenation and rise of the Ediacaran biota in the middle Ediacaran are in agreement with previous studies based on analyses of Mo-U-S-Tl isotopes suggesting that a significant ocean oxygenation event may have happened during the SE and that the increase in global ocean oxygenation likely triggered the evolution of the Ediacaran-type biota [3,67,76,77].

Moreover, existing observations have revealed an anoxia-dominated global deep ocean and a highly redox-stratified shelf ocean during the Ediacaran–early Cambrian, in which a mid-depth euxinic (i.e., anoxic and H_2S-bearing or sulfidic) water mass coexisted dynamically with the oxic surface and ferruginous deep waters [78]. Because early animals mainly or exclusively occupied continental shelves [79,80], the dynamically developed mid-depth euxinic waters in the shelf oceans may have extremely shaped the local ecosystems of early animals [66]. Our results suggest that the proportion of euxinic samples show variations of 0.14, 0.07, and 0.19, respectively, which reached their maximum proportion (0.19) in the upper Ediacaran (560–541 Ma) (Figure 4D). The decline of the Ediacaran biota may have been caused by the expansion of the mid-depth euxinic waters in the upper

Ediacaran, whereas more detailed redox and paleontological studies are needed to prove this hypothesis.

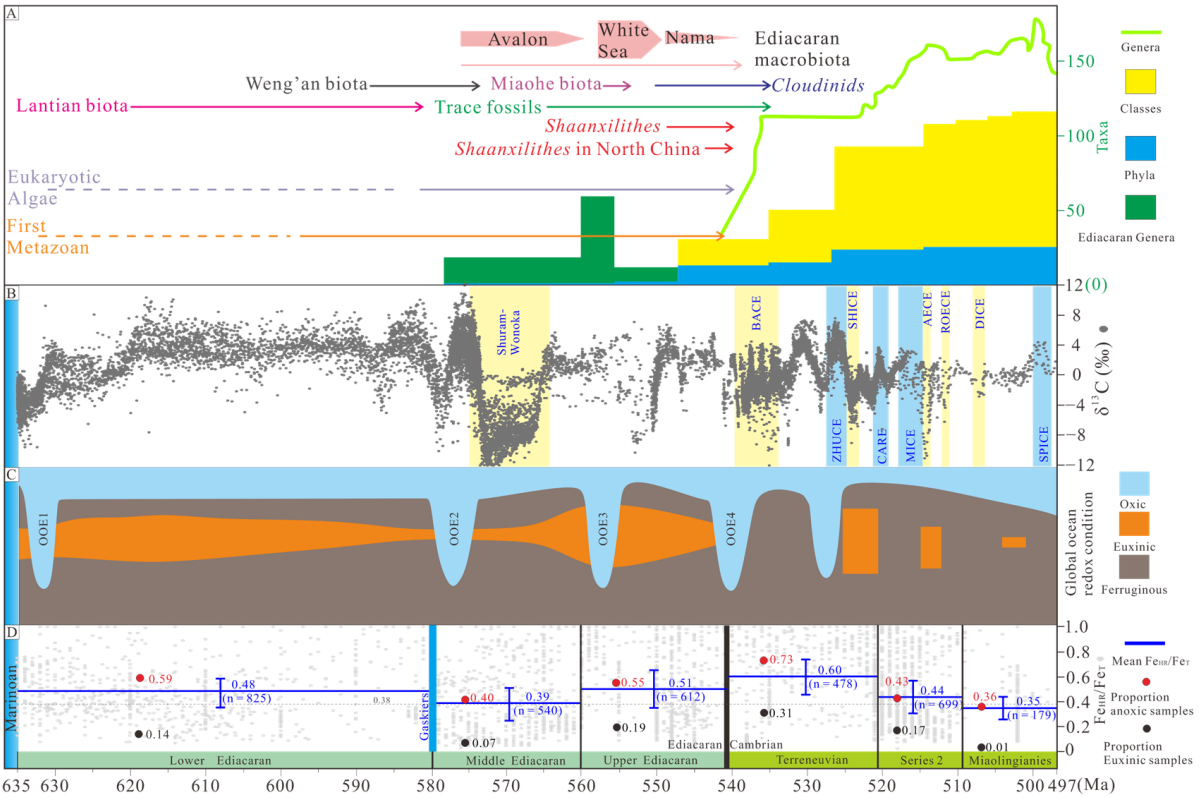


Figure 4. Integrated biotic and geochemical records during 635–497 Ma. (**A**) Fossil ranges and known fossil records of animals at the genus, class, and phylum levels, modified from [62,69,81]. Ediacaran genera are the generic record of macroscopic Ediacara fossils. (**B**) Integrated carbon isotopic profile, modified from [6,61,82]. (**C**) Schematic evolution of global redox conditions, modified from complied iron speciation data in D and [83]. (**D**) Mean Fe_{HR}/Fe_T ratios from the global iron speciation database (635–497 Ma; Table S2), collected from [9,10,13,50,53,55,60,64,71,84–120]. The proportion of anoxic samples was calculated as the proportion of samples with $Fe_{HR}/Fe_T > 0.38$, and the proportion of euxinic samples was calculated as the proportion of samples with $Fe_{HR}/Fe_T > 0.38$ and $Fe_{Py}/Fe_{HR} > 0.7$. Whiskers represent standard errors. The ages for the Ediacaran are based on subdivision models in [62], and the Cambrian ages are based on the international chronostratigraphic chart.

Additionally, for the early–middle Cambrian, all the mean Fe_{HR}/Fe_T ratios (0.6, 0.44, and 0.35), the proportion of anoxic samples (0.73, 0.43, and 0.36), and the proportion of euxinic samples (0.31, 0.17, and 0.01) show a progressive decline from Terreneuvian to Miaolingian, which may reflect stepwise oxygenation of the early–middle Cambrian ocean (Figure 4D). Corresponding to the stepwise oceanic oxygenation, the number of animals rose dramatically (Figure 4A). Previous studies in South China have found that the expansion of complex arthropod-dominated biotas and the regional increase in the diversity of basic metazoan body plans are consistent with the rising oceanic oxygen levels in the early–middle Cambrian [55]. Our study confirms that this coupled early–middle Cambrian ocean oxygenation and metazoan diversification should be a global phenomenon. Collectively, statistical analysis of global iron speciation data from the Ediacaran to the middle Cambrian revealed dynamic Ediacaran marine redox conditions and stepwise oceanic oxygenation during the early–middle Cambrian. Our findings reinforce previous studies suggesting that the coupled global ocean oxygenation and rise of the Ediacaran biota occurred during the middle Ediacaran and that stepwise oceanic oxygenation may have facilitated the evolution of animals during the early–middle Cambrian.

5. Conclusions

This study presents the detailed geochemical reconstruction of the fossiliferous Ediacaran section across the southern margin of the North China Craton. Iron and RSTEs geochemical data revealed a dominantly anoxic late Ediacaran ocean punctuated by multiple transient oxygenation events across the southern margin of the NCC. This is in agreement with previous studies suggesting that the Ediacaran Period was characterized via the pulsed oxygenation of a predominately anoxic global ocean. Moreover, the new Fe_{HR}/Fe_T and Fe_T/Al data presented here suggest the transient oxidation of shallow oceans during the deposition of the fossiliferous part of the Dongpo Formation. These transient oxidation events in the NCC may have contributed to the appearance of the Ediacaran tubular fossil *Shaanxilithes*. To further assess the relationship between global ocean redox conditions and the evolution of early animals, we integrated our iron speciation data with published data from Ediacaran–middle Cambrian sections in other continents. Statistical analysis of global iron speciation data suggested dynamic Ediacaran marine redox conditions and stepwise oceanic oxygenation during the early–middle Cambrian. Integrated biotic and geochemical records suggested that the coupled global ocean oxygenation and rise of the Ediacaran biota occurred in the middle Ediacaran and that the stepwise early–middle Cambrian ocean oxygenation may have facilitated the evolution of animals.

Supplementary Materials: The following supporting information can be downloaded at: https://www.mdpi.com/article/10.3390/min13091124/s1, Table S1: Fe-redox-sensitive trace elements geochemical data for the Luoquancun section, North China; Table S2: Global iron speciation data from 635 to 497 Ma.

Author Contributions: Investigation, L.W.; data curation, J.Y.; writing—original draft preparation, J.Y.; writing—review and editing, J.Y., W.J., G.W., L.W. and Z.Z.; funding acquisition, J.Y. All authors have read and agreed to the published version of the manuscript.

Funding: This study was supported by the Shandong Provincial Natural Science Foundation (ZR2021QD114) and the Shandong Postdoctoral Program for Innovative Talents (SDBX2020011).

Data Availability Statement: All data generated and analyzed during this study are included in this published article.

Acknowledgments: We appreciate Yuansheng Du, Zuozhen Han, Hongwei Kuang, Yongqing Liu, and Xiaoshuai Chen for their helpful discussions and Chao Li and Zihu Zhang for their iron speciation analyses.

Conflicts of Interest: The authors declare no conflict of interest.

References

1. Lyons, T.W.; Reinhard, C.T.; Planavsky, N.J. The rise of oxygen in Earth's early ocean and atmosphere. *Nature* **2014**, *506*, 307–315. [CrossRef] [PubMed]
2. Holland, H.D. Volcanic gases, black smokers, and the Great Oxidation Event. *Geochim. Cosmochim. Acta* **2002**, *66*, 3811–3826. [CrossRef]
3. Scott, C.; Lyons, T.W.; Bekker, A.; Shen, Y.; Poulton, S.W.; Chu, X.; Anbar, A.D. Tracing the stepwise oxygenation of the Proterozoic ocean. *Nature* **2008**, *452*, 456–459. [CrossRef] [PubMed]
4. Liu, X.; Kah, L.C.; Knoll, A.H.; Cui, H.; Wang, C.; Bekker, A.; Hazen, R.M. A persistently low level of atmospheric oxygen in Earth's middle age. *Nat. Commun.* **2021**, *12*, 351. [CrossRef] [PubMed]
5. Bowyer, F.; Wood, R.A.; Poulton, S.W. Controls on the evolution of Ediacaran metazoan ecosystems: A redox perspective. *Geobiology* **2017**, *15*, 516–551. [CrossRef]
6. Wood, R.; Liu, A.G.; Bowyer, F.; Wilby, P.R.; Dunn, F.S.; Kenchington, C.G.; Cuthill, J.F.H.; Mitchell, E.G.; Penny, A. Integrated records of environmental change and evolution challenge the Cambrian Explosion. *Nat. Ecol. Evol.* **2019**, *3*, 528–538. [CrossRef]
7. Tostevin, R.; Clarkson, M.O.; Gangl, S.; Shields, G.A.; Wood, R.A.; Bowyer, F.; Penny, A.M.; Stirling, C.H. Uranium isotope evidence for an expansion of anoxia in terminal Ediacaran oceans. *Earth. Planet. Sci. Lett.* **2019**, *506*, 104–112. [CrossRef]
8. Zhang, F.; Xiao, S.; Kendall, B.; Romaniello, S.J.; Cui, H.; Meyer, M.; Gilleaudeau, G.J.; Kaufman, A.J.; Anbar, A.D. Extensive marine anoxia during the terminal Ediacaran Period. *Sci. Adv.* **2018**, *4*, eaan8983. [CrossRef]
9. Johnston, D.T.; Poulton, S.W.; Tosca, N.J.; O'Brien, T.; Halverson, G.P.; Schrag, D.P.; Macdonald, F.A. Searching for an oxygenation event in the fossiliferous Ediacaran of northwestern Canada. *Chem. Geol.* **2013**, *362*, 273–286. [CrossRef]

10. Johnston, D.; Poulton, S.W.; Goldberg, T.; Sergeev, V.; Podkovyrov, V.; Vorob'eva, N.G.; Bekker, A.; Knoll, A. Late Ediacaran redox stability and metazoan evolution. *Earth. Planet. Sci. Lett.* **2012**, *335–336*, 25–35. [CrossRef]
11. Macdonald, F.A.; Strauss, J.V.; Sperling, E.A.; Halverson, G.P.; Narbonne, G.M.; Johnston, D.T.; Kunzmann, M.; Schrag, D.P.; Higgins, J.A. The stratigraphic relationship between the Shuram carbon isotope excursion, the oxygenation of Neoproterozoic oceans, and the first appearance of the Ediacara biota and bilaterian trace fossils in northwestern Canada. *Chem. Geol.* **2013**, *362*, 250–272. [CrossRef]
12. Ostrander, C.M.; Owens, J.D.; Nielsen, S.G.; Lyons, T.W.; Shu, Y.; Chen, X.; Sperling, E.A.; Jiang, G.; Johnston, D.T.; Sahoo, S.K.; et al. Thallium isotope ratios in shales from South China and northwestern Canada suggest widespread O2 accumulation in marine bottom waters was an uncommon occurrence during the Ediacaran Period. *Chem. Geol.* **2020**, *557*, 119856. [CrossRef]
13. Miller, A.J.; Strauss, J.V.; Halverson, G.P.; Macdonald, F.A.; Johnston, D.T.; Sperling, E.A. Tracking the onset of Phanerozoic-style redox-sensitive trace metal enrichments: New results from basal Ediacaran post-glacial strata in NW Canada. *Chem. Geol.* **2017**, *457*, 24–37. [CrossRef]
14. Li, Z.X.; Evans, D.A.; Halverson, G.P. Neoproterozoic glaciations in a revised global palaeogeography from the breakup of Rodinia to the assembly of Gondwanaland. *Sediment. Geol.* **2013**, *294*, 219–232. [CrossRef]
15. Zhao, G.; Wang, Y.; Huang, B.; Dong, Y.; Li, S.; Zhang, G.; Yu, S. Geological reconstructions of the East Asian blocks: From the breakup of Rodinia to the assembly of Pangea. *Earth-Sci. Rev.* **2018**, *186*, 262–286. [CrossRef]
16. Wen, B.; Evans, D.A.D.; Li, Y.-X. Neoproterozoic paleogeography of the Tarim Block: An extended or alternative "missing-link" model for Rodinia? *Earth. Planet. Sci. Lett.* **2017**, *458*, 92–106. [CrossRef]
17. Merdith, A.S.; Collins, A.S.; Williams, S.E.; Pisarevsky, S.; Foden, J.D.; Archibald, D.B.; Blades, M.L.; Alessio, B.L.; Armistead, S.; Plavsa, D.; et al. A full-plate global reconstruction of the Neoproterozoic. *Gondwana Res.* **2017**, *50*, 84–134. [CrossRef]
18. Zhao, G.; Wilde, S.A.; Cawood, P.A.; Sun, M. Archean blocks and their boundaries in the North China Craton: Lithological, geochemical, structural and P–T path constraints and tectonic evolution. *Precambrian Res.* **2001**, *107*, 45–73. [CrossRef]
19. Hu, J.; Gong, W.; Wu, S.; Liu, Y.; Liu, S. LA-ICP-MS zircon U–Pb dating of the Langshan Group in the northeast margin of the Alxa block, with tectonic implications. *Precambrian Res.* **2014**, *255*, 756–770. [CrossRef]
20. Deng, Y.; Wang, H.; Lyu, D.; Zhang, F.; Gao, Z.; Ren, R.; Ye, Y.; Lyu, Y.; Wang, X.; Guan, P.; et al. Evolution of the 1.8–1.6 Ga Yanliao and Xiong'er basins, north China Craton. *Precambrian Res.* **2021**, *365*, 106383. [CrossRef]
21. Liu, D.Y.; Nutman, A.P.; Compston, W.; Wu, J.S.; Shen, Q.H. Remnants of ≥3800 Ma crust in the Chinese part of the Sino-Korean craton. *Geology* **1992**, *20*, 339. [CrossRef]
22. Zhao, G.; Cawood, P.A. Precambrian geology of China. *Precambrian Res.* **2012**, *222*, 13–54. [CrossRef]
23. Yang, J.; Zhu, Q.; Zeng, Z.; Wan, L. Zircon U–Pb ages and Hf isotope compositions of the Neoproterozoic magmatic rocks in the Helan Mountains, North China. *Geol. Mag.* **2019**, *156*, 2104–2112. [CrossRef]
24. Zuo, P.; Li, Y.; Zhang, G.; Si, R.; Wang, S.; Liu, S.; Zheng, D.; Sun, J. Reviews of the Mesoproterozoic to Neoproterozoic sedimentary sequences and new constraints on the tectono-sedimentary evolution of the southern margin of the North China Craton. *J. Asian Earth Sci.* **2019**, *179*, 416–429. [CrossRef]
25. Zhong, Y.; Zhai, M.; Peng, P.; Santosh, M.; Ma, X. Detrital zircon U–Pb dating and whole-rock geochemistry from the clastic rocks in the northern marginal basin of the North China Craton: Constraints on depositional age and provenance of the Bayan Obo Group. *Precambrian Res.* **2015**, *258*, 133–145. [CrossRef]
26. Li, M.; Vandyk, T.M.; Wu, G.; Liu, W.; Le Heron, D.P.; Xiao, Y. A window into the Great Unconformity: Insights from geochemistry and geochronology of Ediacaran glaciogenic rocks in the North China Craton. *J. Asian Earth Sci.* **2020**, *194*, 104327. [CrossRef]
27. Yang, J.; Lyons, T.W.; Zeng, Z.; Odigie, K.O.; Bates, S.; Hu, L. Geochemical constraints on the origin of Neoproterozoic cap carbonate in the Helan Mountains, North China: Implications for mid-late Ediacaran glaciation? *Precambrian Res.* **2019**, *331*, 105361. [CrossRef]
28. Dong, X.P.; Hu, J.M.; Li, Z.H.; Zhao, Y.; Gong, W.B.; Yang, Y. Provenance of Ediacaran (Sinian) sediments in the Helanshan area, North China Craton: Constraints from U–Pb geochronology and Hf isotopes of detrital zircons. *Precambrian Res.* **2017**, *298*, 490–511. [CrossRef]
29. Yang, J.; Zeng, Z.; Cai, X.; Li, Z.; Li, T.; Meng, F.; He, W. Carbon and oxygen isotopes analyses for the Sinian carbonates in the Helan Mountain, North China. *Chin. Sci. Bull.* **2013**, *58*, 3943–3955. [CrossRef]
30. Chen, X.; Kuang, H.; Liu, Y.; Wang, Y.; Yang, Z.; Vandyk, T.M.; Le Heron, D.P.; Wang, S.; Geng, Y.; Bai, H.; et al. Subglacial bedforms and landscapes formed by an ice sheet of Ediacaran-Cambrian age in west Henan, North China. *Precambrian Res.* **2020**, *344*, 105727. [CrossRef]
31. Wang, X.; Zhang, X.; Liu, W. Biostratigraphic constraints on the age of Neoproterozoic glaciation in North China. *J. Asian Earth Sci.* **2021**, *219*, 104894. [CrossRef]
32. Wang, X.; Zhang, X.; Zhang, Y.; Cui, L.; Li, L. New materials reveal *Shaanxilithes* as a *Cloudina*-like organism of the late Ediacaran. *Precambrian Res.* **2021**, *362*, 106277. [CrossRef]
33. Shen, B.; Xiao, S.; Dong, L.; Zhou, C.; Liu, J. Problematic macrofossils from Ediacaran successions in the North China and Chaidam blocks: Implications for their evolutionary roots and biostratigraphic significance. *J. Paleontol.* **2007**, *81*, 1396–1411. [CrossRef]
34. Chai, S.; Wu, Y.; Hua, H. Potential index fossils for the Terminal Stage of the Ediacaran System. *J. Asian Earth Sci.* **2021**, *218*, 104885. [CrossRef]

35. Pang, K.; Wu, C.; Sun, Y.; Ouyang, Q.; Yuan, X.; Shen, B.; Lang, X.; Wang, R.; Chen, Z.; Zhou, C. New Ediacara-type fossils and late Ediacaran stratigraphy from the northern Qaidam Basin (China): Paleogeographic implications. *Geology* **2021**, *49*, 1160–1164. [CrossRef]
36. Le Heron, D.P.; Vandyk, T.M.; Kuang, H.; Liu, Y.; Chen, X.; Wang, Y.; Yang, Z.; Scharfenberg, L.; Davies, B.; Shields, G. Bird's-eye view of an Ediacaran subglacial landscape. *Geology* **2019**, *47*, 705–709. [CrossRef]
37. Zhang, B.; Zheng, D. Sedimentological, geochemical, and geochronological constraints on the origin of the Neoproterozoic Luoquan Formation at the Southern Margin of the North China Craton. *Int. Geol. Rev.* **2021**, *64*, 911–932. [CrossRef]
38. Guan, B.; Ruitang, W.U.; Hambrey, M.J.; Geng, W. Glacial sediments and erosional pavements near the Cambrian-Precambrian boundary in western Henan Province, China. *J. Geol. Soc.* **1986**, *143*, 311–323.
39. Wedepohl, K.H. Environmental influences on the chemical composition of shales and clays. *Phys. Chem. Earth* **1971**, *8*, 307–333. [CrossRef]
40. Poulton, S.W.; Canfield, D.E. Development of a sequential extraction procedure for iron: Implications for iron partitioning in continentally derived particulates. *Chem. Geol.* **2005**, *214*, 209–221. [CrossRef]
41. Canfield, D.E.; Raiswell, R.; Westrich, J.T.; Reaves, C.M.; Berner, R.A. The use of chromium reduction in the analysis of reduced inorganic sulfur in sediments and shales. *Chem. Geol.* **1986**, *54*, 149–155. [CrossRef]
42. Poulton, S.W.; Canfield, D.E. Ferruginous Conditions: A Dominant Feature of the Ocean through Earth's History. *Elements* **2011**, *7*, 107–112. [CrossRef]
43. Raiswell, R.; Canfield, D.E. Sources of iron for pyrite formation in marine sediments. *Am. J. Sci.* **1998**, *298*, 219–245. [CrossRef]
44. Li, C.; Love, G.D.; Lyons, T.W.; Scott, C.T.; Feng, L.; Huang, J.; Chang, H.; Zhang, Q.; Chu, X. Evidence for a redox stratified Cryogenian marine basin, Datangpo Formation, South China. *Earth. Planet. Sci. Lett.* **2012**, *331–332*, 246–256. [CrossRef]
45. Lyons, T.W.; Severmann, S. A critical look at iron paleoredox proxies: New insights from modern euxinic marine basins. *Geochim. Cosmochim. Acta* **2006**, *70*, 5698–5722. [CrossRef]
46. Raiswell, R.; Hardisty, D.S.; Lyons, T.W.; Canfield, D.E.; Owens, J.D.; Planavsky, N.J.; Poulton, S.W.; Reinhard, C.T. The iron paleoredox proxies: A guide to the pitfalls, problems and proper practice. *Am. J. Sci.* **2018**, *318*, 491–526. [CrossRef]
47. Clarkson, M.O.; Poulton, S.W.; Guilbaud, R.; Wood, R.A. Assessing the utility of Fe/Al and Fe-speciation to record water column redox conditions in carbonate-rich sediments. *Chem. Geol.* **2014**, *382*, 111–122. [CrossRef]
48. Sperling, E.A.; Halverson, G.P.; Knoll, A.H.; Macdonald, F.A.; Johnston, D.T. A basin redox transect at the dawn of animal life. *Earth. Planet. Sci. Lett.* **2013**, *371–372*, 143–155. [CrossRef]
49. Bridger, P.; Poulton, S.W.; Zhou, Y.; Li, C.; Zhang, K.; Shields, G.A. The Ediacaran 'Miaohe Member' of South China: New insights from palaeoredox proxies and stable isotope data. *Geol. Mag.* **2021**, *159*, 1014–1028. [CrossRef]
50. Sperling, E.A.; Carbone, C.; Strauss, J.V.; Johnston, D.T.; Narbonne, G.M.; Macdonald, F.A. Oxygen, facies, and secular controls on the appearance of Cryogenian and Ediacaran body and trace fossils in the Mackenzie Mountains of northwestern Canada. *Geol. Soc. Am. Bull.* **2015**, *128*, 558–575. [CrossRef]
51. Uahengo, C.-I.; Shi, X.; Jiang, G.; Vatuva, A. Transient shallow-ocean oxidation associated with the late Ediacaran Nama skeletal fauna: Evidence from iodine contents of the Lower Nama Group, southern Namibia. *Precambrian Res.* **2020**, *343*, 105732. [CrossRef]
52. Cheng, M.; Zhang, Z.; Algeo, T.J.; Liu, S.; Liu, X.; Wang, H.; Chang, B.; Jin, C.; Pan, W.; Cao, M.; et al. Hydrological controls on marine chemistry in the Cryogenian Nanhua Basin (South China). *Earth-Sci. Rev.* **2021**, *218*, 103678. [CrossRef]
53. Jin, C.; Li, C.; Algeo, T.J.; O'Connell, B.; Cheng, M.; Shi, W.; Shen, J.; Planavsky, N.J. Highly heterogeneous "poikiloredox" conditions in the early Ediacaran Yangtze Sea. *Precambrian Res.* **2018**, *311*, 157–166. [CrossRef]
54. Helz, G.R.; Miller, C.V.; Charnock, J.M.; Mosselmans, J.F.W.; Pattrick, R.A.D.; Garner, C.D.; Vaughan, D.J. Mechanism of molybdenum removal from the sea and its concentration in black shales: EXAFS evidence. *Geochim. Cosmochim. Acta* **1996**, *60*, 3631–3642. [CrossRef]
55. Li, C.; Jin, C.; Planavsky, N.J.; Algeo, T.J.; Cheng, M.; Yang, X.; Zhao, Y.; Xie, S. Coupled oceanic oxygenation and metazoan diversification during the early–middle Cambrian? *Geology* **2017**, *45*, 743–746. [CrossRef]
56. Reinhard, C.T.; Planavsky, N.J.; Robbins, L.J.; Partin, C.A.; Gill, B.C.; Lalonde, S.V.; Bekker, A.; Konhauser, K.O.; Lyons, T.W. Proterozoic ocean redox and biogeochemical stasis. *Proc. Natl. Acad. Sci. USA* **2013**, *110*, 5357–5362. [CrossRef]
57. Och, L.M.; Shields-Zhou, G.A. The Neoproterozoic oxygenation event: Environmental perturbations and biogeochemical cycling. *Earth-Sci. Rev.* **2012**, *110*, 26–57. [CrossRef]
58. Wang, H.; Liu, A.; Li, C.; Feng, Q.; Tang, S.; Cheng, M.; Algeo, T.J. A benthic oxygen oasis in the early Neoproterozoic ocean. *Precambrian Res.* **2021**, *355*, 106085. [CrossRef]
59. Scott, C.; Lyons, T.W. Contrasting molybdenum cycling and isotopic properties in euxinic versus non-euxinic sediments and sedimentary rocks: Refining the paleoproxies. *Chem. Geol.* **2012**, *324–325*, 19–27. [CrossRef]
60. Sahoo, S.; Planavsky, N.; Jiang, G.; Kendall, B.; Owens, J.; Wang, X.; Shi, X.; Anbar, A.; Lyons, T. Oceanic oxygenation events in the anoxic Ediacaran ocean. *Geobiology* **2016**, *14*, 457–468. [CrossRef]
61. Yang, C.; Rooney, A.D.; Condon, D.J.; Li, X.-H.; Grazhdankin, D.V.; Bowyer, F.T.; Hu, C.; Macdonald, F.A.; Zhu, M. The tempo of Ediacaran evolution. *Sci. Adv.* **2021**, *7*, eabi9643. [CrossRef] [PubMed]
62. Xiao, S.; Narbonne, G.M.; Zhou, C.; Laflamme, M.; Grazhdankin, D.V. Towards an Ediacaran Time Scale: Problems, Protocols, and Prospects. *Episodes* **2016**, *39*, 540–555. [CrossRef]

63. Tostevin, R.; Wood, R.; Shields, G.; Poulton, S.; Guilbaud, R.; Bowyer, F.; Penny, A.; He, T.; Curtis, A.; Hoffmann, K. Low-oxygen waters limited habitable space for early animals. *Nat. Commun.* **2016**, *7*, 12818. [CrossRef]
64. Wood, R.A.; Poulton, S.W.; Prave, A.R.; Hoffmann, K.H.; Clarkson, M.O.; Guilbaud, R.; Lyne, J.W.; Tostevin, R.; Bowyer, F.; Penny, A.M.; et al. Dynamic redox conditions control late Ediacaran metazoan ecosystems in the Nama Group, Namibia. *Precambrian Res.* **2015**, *261*, 252–271. [CrossRef]
65. Tostevin, R.; He, T.; Turchyn, A.V.; Wood, R.A.; Penny, A.M.; Bowyer, F.; Antler, G.; Shields, G.A. Constraints on the late Ediacaran sulfur cycle from carbonate associated sulfate. *Precambrian Res.* **2017**, *290*, 113–125. [CrossRef]
66. Li, C.; Cheng, M.; Zhu, M.; Lyons, T.W. Heterogeneous and dynamic marine shelf oxygenation and coupled early animal evolution. *Emerg. Top. Life Sci.* **2018**, *2*, 279–288. [CrossRef]
67. Zhang, F.; Xiao, S.; Romaniello, S.; Hardisty, D.S.; Li, C.; Melezhik, V.; Pokrovsky, B.; Cheng, M.; Shi, W.; Lenton, T.M.; et al. Global marine redox changes drove the rise and fall of the Ediacara biota. *Geobiology* **2019**, *17*, 594–610. [CrossRef]
68. Evans, S.D.; Diamond, C.W.; Droser, M.L.; Lyons, T.W. Dynamic oxygen and coupled biological and ecological innovation during the second wave of the Ediacara Biota. *Emerg. Top. Life Sci.* **2018**, *2*, 223–233. [CrossRef]
69. Wei, G.; Planavsky, N.J.; He, T.; Zhang, F.; Stockey, R.G.; Cole, D.B.; Lin, Y.; Ling, H. Global marine redox evolution from the late Neoproterozoic to the early Paleozoic constrained by the integration of Mo and U isotope records. *Earth-Sci. Rev.* **2021**, *214*, 103506. [CrossRef]
70. Fike, D.A.; Grotzinger, J.P.; Pratt, L.M.; Summons, R.E. Oxidation of the Ediacaran Ocean. *Nature* **2006**, *444*, 744–747. [CrossRef]
71. Sperling, E.A.; Wolock, C.J.; Morgan, A.S.; Gill, B.C.; Kunzmann, M.; Halverson, G.P.; Macdonald, F.A.; Knoll, A.H.; Johnston, D.T. Statistical analysis of iron geochemical data suggests limited late Proterozoic oxygenation. *Nature* **2015**, *523*, 451–454. [CrossRef]
72. Xiao, S.; Laflamme, M. On the eve of animal radiation: Phylogeny, ecology and evolution of the Ediacara biota. *Trends Ecol. Evol.* **2009**, *24*, 31–40. [CrossRef] [PubMed]
73. Darroch, S.A.F.; Smith, E.F.; Laflamme, M.; Erwin, D.H. Ediacaran Extinction and Cambrian Explosion. *Trends Ecol. Evol.* **2018**, *33*, 653–663. [CrossRef] [PubMed]
74. Shen, B.; Dong, L.; Xiao, S.; Kowalewski, M. The Avalon explosion: Evolution of Ediacara morphospace. *Science* **2008**, *319*, 81–84. [CrossRef] [PubMed]
75. Laflamme, M.; Darroch, S.A.F.; Tweedt, S.M.; Peterson, K.J.; Erwin, D.H. The end of the Ediacara biota: Extinction, biotic replacement, or Cheshire Cat? *Gondwana Res.* **2013**, *23*, 558–573. [CrossRef]
76. Mcfadden, K.A.; Huang, J.; Chu, X.; Jiang, G.; Kaufman, A.J.; Zhou, C.; Yuan, X.; Xiao, S. Pulsed oxidation and biological evolution in the Ediacaran Doushantuo Formation. *Proc. Natl. Acad. Sci. USA* **2008**, *105*, 3197–3202. [CrossRef]
77. Fan, H.; Nielsen, S.G.; Owens, J.D.; Auro, M.; Shu, Y.; Hardisty, D.S.; Horner, T.J.; Bowman, C.N.; Young, S.A.; Wen, H. Constraining oceanic oxygenation during the Shuram excursion in South China using thallium isotopes. *Geobiology* **2020**, *18*, 348–365. [CrossRef]
78. Li, C.; Shi, W.; Cheng, M.; Jin, C.; Algeo, T.J. The redox structure of Ediacaran and early Cambrian oceans and its controls. *Sci. Bull.* **2020**, *65*, 2141–2149. [CrossRef]
79. Zhu, M. The origin and Cambrian explosion of animals: Fossil evidences from China. *Acta Palaeontol. Sin.* **2010**, *49*, 269–287.
80. Xiao, S.; Chen, Z.; Zhou, C.; Yuan, X. Surfing in and on microbial mats: Oxygen-related behavior of a terminal Ediacaran bilaterian animal. *Geology* **2019**, *47*, 1054–1058. [CrossRef]
81. Erwin, D.H.; Laflamme, M.; Tweedt, S.M.; Sperling, E.A.; Pisani, D.; Peterson, K.J. The Cambrian conundrum: Early divergence and later ecological success in the early history of animals. *Science* **2011**, *334*, 1091. [CrossRef] [PubMed]
82. Bowyer, F.T.; Zhuravlev, A.Y.; Wood, R.; Shields, G.A.; Zhou, Y.; Curtis, A.; Poulton, S.W.; Condon, D.J.; Yang, C.; Zhu, M. Calibrating the temporal and spatial dynamics of the Ediacaran—Cambrian radiation of animals. *Earth-Sci. Rev.* **2022**, *225*, 103913. [CrossRef]
83. Wood, R.; Donoghue, P.C.J.; Lenton, T.M.; Liu, A.G.; Poulton, S.W. The origin and rise of complex life: Progress requires interdisciplinary integration and hypothesis testing. *Interface Focus* **2020**, *10*, 20200024. [CrossRef]
84. Zhu, B.; Yang, T.; Wang, J.; Chen, X.; Pan, W.; Chen, Y. Multiple controls on the paleoenvironment of the early Cambrian black shale-chert in the northwest Tarim Basin, NW China: Trace element, iron speciation and Mo isotopic evidence. *Mar. Pet. Geol.* **2022**, *136*, 105434. [CrossRef]
85. Zhu, G.; Li, T.; Zhao, K.; Li, C.; Cheng, M.; Chen, W.; Yan, H.; Zhang, Z.; Algeo, T.J. Mo isotope records from Lower Cambrian black shales, northwestern Tarim Basin (China): Implications for the early Cambrian ocean. *GSA Bull.* **2021**, *134*, 3–14. [CrossRef]
86. Zhang, Z.; Li, C.; Cheng, M.; Algeo, T.J.; Jin, C.; Tang, F.; Huang, J. Evidence for Highly Complex Redox Conditions and Strong Water-Column Stratification in an Early Cambrian Continental-Margin Sea. *Geochem. Geophys. Geosyst.* **2018**, *19*, 2397–2410. [CrossRef]
87. Yuan, Y.; Cai, C.; Wang, T.; Xiang, L.; Jia, L.; Chen, Y. Redox condition during Ediacaran–Cambrian transition in the Lower Yangtze deep water basin, South China: Constraints from iron speciation and δ13Corg in the Diben section, Zhejiang. *Chin. Sci. Bull.* **2014**, *59*, 3638–3649. [CrossRef]
88. Ye, Y.; Wang, H.; Wang, X.; Zhai, L.; Wu, C.; Canfield, D.E.; Zhang, S. Tracking the evolution of seawater Mo isotopes through the Ediacaran–Cambrian transition. *Precambrian Res.* **2020**, *350*, 105929. [CrossRef]

89. Xu, L.; Lehmann, B.; Mao, J.; Nägler, T.F.; Neubert, N.; Böttcher, M.E.; Escher, P. Mo isotope and trace element patterns of Lower Cambrian black shales in South China: Multi-proxy constraints on the paleoenvironment. *Chem. Geol.* **2012**, *318–319*, 45–59. [CrossRef]
90. Xiang, L.; Schoepfer, S.D.; Shen, S.-Z.; Cao, C.-Q.; Zhang, H. Evolution of oceanic molybdenum and uranium reservoir size around the Ediacaran–Cambrian transition: Evidence from western Zhejiang, South China. *Earth. Planet. Sci. Lett.* **2017**, *464*, 84–94. [CrossRef]
91. Wen, H.; Fan, H.; Zhang, Y.; Cloquet, C.; Carignan, J. Reconstruction of early Cambrian ocean chemistry from Mo isotopes. *Geochim. Cosmochim. Acta* **2015**, *164*, 1–16. [CrossRef]
92. Wen, H.; Carignan, J.; Chu, X.; Fan, H.; Cloquet, C.; Huang, J.; Zhang, Y.; Chang, H. Selenium isotopes trace anoxic and ferruginous seawater conditions in the Early Cambrian. *Chem. Geol.* **2014**, *390*, 164–172. [CrossRef]
93. Wang, J.; Chen, D.; Yan, D.; Wei, H.; Xiang, L. Evolution from an anoxic to oxic deep ocean during the Ediacaran–Cambrian transition and implications for bioradiation. *Chem. Geol.* **2012**, *306–307*, 129–138. [CrossRef]
94. Sahoo, S.K.; Planavsky, N.J.; Kendall, B.; Wang, X.; Shi, X.; Scott, C.; Anbar, A.D.; Lyons, T.W.; Jiang, G. Ocean oxygenation in the wake of the Marinoan glaciation. *Nature* **2012**, *489*, 546. [CrossRef]
95. Ostrander, C.M.; Sahoo, S.K.; Kendall, B.; Jiang, G.; Planavsky, N.J.; Lyons, T.W.; Nielsen, S.G.; Owens, J.D.; Gordon, G.W.; Romaniello, S.J.; et al. Multiple negative molybdenum isotope excursions in the Doushantuo Formation (South China) fingerprint complex redox-related processes in the Ediacaran Nanhua Basin. *Geochim. Cosmochim. Acta* **2019**, *261*, 191–209. [CrossRef]
96. Och, L.M.; Cremonese, L.; Shields-Zhou, G.A.; Poulton, S.W.; Struck, U.; Ling, H.; Li, D.; Chen, X.; Manning, C.; Thirlwall, M.; et al. Palaeoceanographic controls on spatial redox distribution over the Yangtze Platform during the Ediacaran–Cambrian transition. *Sedimentology* **2016**, *63*, 378–410. [CrossRef]
97. Liu, Y.; Magnall, J.M.; Gleeson, S.A.; Bowyer, F.; Poulton, S.W.; Zhang, J. Spatio-temporal evolution of ocean redox and nitrogen cycling in the early Cambrian Yangtze ocean. *Chem. Geol.* **2020**, *554*, 119803. [CrossRef]
98. Li, C.; Planavsky, N.J.; Shi, W.; Zhang, Z.; Zhou, C.; Cheng, M.; Tarhan, L.G.; Luo, G.; Xie, S. Ediacaran Marine Redox Heterogeneity and Early Animal Ecosystems. *Sci. Rep.* **2015**, *5*, 17097. [CrossRef]
99. Li, C.; Love, G.D.; Lyons, T.W.; Fike, D.A.; Sessions, A.L.; Chu, X. A Stratified Redox Model for the Ediacaran Ocean. *Science* **2010**, *328*, 80–83. [CrossRef]
100. Kunzmann, M.; Halverson, G.P.; Scott, C.; Minarik, W.G.; Wing, B.A. Geochemistry of Neoproterozoic black shales from Svalbard: Implications for oceanic redox conditions spanning Cryogenian glaciations. *Chem. Geol.* **2015**, *417*, 383–393. [CrossRef]
101. Kendall, B.; Komiya, T.; Lyons, T.W.; Bates, S.M.; Gordon, G.W.; Romaniello, S.J.; Jiang, G.; Creaser, R.A.; Xiao, S.; McFadden, K.; et al. Uranium and molybdenum isotope evidence for an episode of widespread ocean oxygenation during the late Ediacaran Period. *Geochim. Cosmochim. Acta* **2015**, *156*, 173–193. [CrossRef]
102. Jin, C.; Li, C.; Algeo, T.J.; Planavsky, N.J.; Cui, H.; Yang, X.; Zhao, Y.; Zhang, X.; Xie, S. A highly redox-heterogeneous ocean in South China during the early Cambrian (~529–514 Ma): Implications for biota-environment co-evolution. *Earth. Planet. Sci. Lett.* **2016**, *441*, 38–51. [CrossRef]
103. Huang, J.; Feng, L.; Chu, X.; Sun, T.; Wen, H.; Qin, L.; Shen, Y. A predominantly ferruginous condition in the Ediacaran deep ocean: Geochemistry of black shales in the Ediacaran Doushantuo Formation, South China. *Precambrian Res.* **2017**, *295*, 12–23. [CrossRef]
104. Hippertt, J.P.; Caxito, F.A.; Uhlein, G.J.; Nalini, H.A.; Sial, A.N.; Abreu, A.T.; Nogueira, L.B. The fate of a Neoproterozoic intracratonic marine basin: Trace elements, TOC and IRON speciation geochemistry of the Bambuí Basin, Brazil. *Precambrian Res.* **2019**, *330*, 101–120. [CrossRef]
105. Han, T.; Fan, H. Dynamic evolution of the Ediacaran ocean across the Doushantuo Formation, South China. *Chem. Geol.* **2015**, *417*, 261–272. [CrossRef]
106. Hammarlund, E.U.; Gaines, R.R.; Prokopenko, M.G.; Qi, C.; Hou, X.-G.; Canfield, D.E. Early Cambrian oxygen minimum zone-like conditions at Chengjiang. *Earth. Planet. Sci. Lett.* **2017**, *475*, 160–168. [CrossRef]
107. Frei, R.; Gaucher, C.; Stolper, D.; Canfield, D.E. Fluctuations in late Neoproterozoic atmospheric oxidation—Cr isotope chemostratigraphy and iron speciation of the late Ediacaran lower Arroyo del Soldado Group (Uruguay). *Gondwana Res.* **2013**, *23*, 797–811. [CrossRef]
108. Feng, L.; Li, C.; Huang, J.; Chang, H.; Chu, X. A sulfate control on marine mid-depth euxinia on the early Cambrian (ca. 529–521 Ma) Yangtze platform, South China. *Precambrian Res.* **2014**, *246*, 123–133. [CrossRef]
109. Fan, H.; Wen, H.; Han, T.; Zhu, X.; Feng, L.; Chang, H. Oceanic redox condition during the late Ediacaran (551–541 Ma), South China. *Geochim. Cosmochim. Acta* **2018**, *238*, 343–356. [CrossRef]
110. Creveling, J.R.; Johnston, D.T.; Poulton, S.W.; Kotrc, B.; März, C.; Schrag, D.P.; Knoll, A.H. Phosphorus sources for phosphatic Cambrian carbonates. *GSA Bull.* **2014**, *126*, 145–163. [CrossRef]
111. Cheng, M.; Li, C.; Jin, C.; Wang, H.; Algeo, T.J.; Lyons, T.W.; Zhang, F.; Anbar, A. Evidence for high organic carbon export to the early Cambrian seafloor. *Geochim. Cosmochim. Acta* **2020**, *287*, 125–140. [CrossRef]
112. Cheng, M.; Li, C.; Zhou, L.; Feng, L.; Algeo, T.J.; Zhang, F.; Romaniello, S.; Jin, C.; Ling, H.; Jiang, S. Transient deep-water oxygenation in the early Cambrian Nanhua Basin, South China. *Geochim. Cosmochim. Acta* **2017**, *210*, 42–58. [CrossRef]

113. Chen, Y.; Huang, J.; Zhong, Y.; Zhang, X.; Zhai, M.; Chu, X. Suboxic-dominated conditions in the Ediacaran shallow ocean: Geochemistry of pelitic siltstones in the Doushantuo Formation, South China. *Palaeogeogr. Palaeoclimatol. Palaeoecol.* **2020**, *546*, 109658. [CrossRef]
114. Chen, X.; Ling, H.-F.; Vance, D.; Shields-Zhou, G.A.; Zhu, M.; Poulton, S.W.; Och, L.M.; Jiang, S.-Y.; Li, D.; Cremonese, L.; et al. Rise to modern levels of ocean oxygenation coincided with the Cambrian radiation of animals. *Nat. Commun.* **2015**, *6*, 7142. [CrossRef] [PubMed]
115. Chang, H.; Chu, X.; Feng, L.; Huang, J.; Chen, Y. Marine redox stratification on the earliest Cambrian (ca. 542–529 Ma) Yangtze Platform. *Palaeogeogr. Palaeoclimatol. Palaeoecol.* **2018**, *504*, 75–85. [CrossRef]
116. Canfield, D.E.; Poulton, S.W.; Knoll, A.H.; Narbonne, G.M.; Ross, G.; Goldberg, T.; Strauss, H. Ferruginous Conditions Dominated Later Neoproterozoic Deep-Water Chemistry. *Science* **2008**, *321*, 949–952. [CrossRef]
117. Canfield, D.E.; Poulton, S.W.; Narbonne, G.M. Late-Neoproterozoic deep-ocean oxygenation and the rise of animal life. *Science* **2007**, *315*, 92–95. [CrossRef]
118. Cai, C.; Xiang, L.; Yuan, Y.; He, X.; Chu, X.; Chen, Y.; Xu, C. Marine C, S and N biogeochemical processes in the redox-stratified early Cambrian Yangtze ocean. *J. Geol. Soc.* **2015**, *172*, 390–406. [CrossRef]
119. Bykova, N.; Gill, B.C.; Grazhdankin, D.; Rogov, V.; Xiao, S. A geochemical study of the Ediacaran discoidal fossil Aspidella preserved in limestones: Implications for its taphonomy and paleoecology. *Geobiology* **2017**, *15*, 572–587. [CrossRef]
120. Bowyer, F.T.; Shore, A.J.; Wood, R.A.; Alcott, L.J.; Thomas, A.L.; Butler, I.B.; Curtis, A.; Hainanan, S.; Curtis-Walcott, S.; Penny, A.M.; et al. Regional nutrient decrease drove redox stabilisation and metazoan diversification in the late Ediacaran Nama Group, Namibia. *Sci. Rep.* **2020**, *10*, 2240. [CrossRef]

Disclaimer/Publisher's Note: The statements, opinions and data contained in all publications are solely those of the individual author(s) and contributor(s) and not of MDPI and/or the editor(s). MDPI and/or the editor(s) disclaim responsibility for any injury to people or property resulting from any ideas, methods, instructions or products referred to in the content.